Femtosecond depolarization of photoluminescence from InAs: Comparison with Cu and monolayer graphene

Takeshi Koyama ,* Akira Fujisaki, Hiromu Odamura, Yuto Nakamura , and Hideo Kishida
Department of Applied Physics, Nagoya University, Chikusa, Nagoya 464-8603, Japan

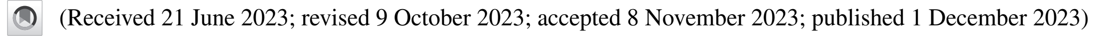

(Received 21 June 2023; revised 9 October 2023; accepted 8 November 2023; published 1 December 2023)

We investigated the time-resolved photoluminescence (PL) of InAs, Cu, and monolayer graphene excited by linearly polarized femtosecond pulses. PL depolarization occurred in the femtosecond regime. The establishment of the isotropic momentum distribution of electrons is discussed based on the electron-electron and electron-phonon scattering. This study demonstrates the impact of a steep dispersion relation in the electron band structure on the electron-optical phonon scattering causing the ultrafast depolarization of PL.

DOI: 10.1103/PhysRevB.108.235103

I. INTRODUCTION

Electronic excitation of solids by photoabsorption generates anisotropic momentum and spin distributions of electrons depending on the light polarization [1]. Excitation with linearly or circularly polarized light results in an anisotropic momentum or spin distribution, respectively. Light polarization can be used as the degree of freedom of light applied to information technology by writing polarization onto materials [2]. For this application, it is important to understand the speed and mechanism of depolarization in materials.

The depolarization is caused by scattering phenomena such as electron-electron and electron-phonon scattering, and it has been studied by observing photoluminescence (PL). For early examples of III-V semiconductors, the depolarization in bulk GaAs and quantum wells has been investigated by measuring steady-state PL [3–6], picosecond PL [7,8], and femtosecond PL [9]. The PL measurements also have revealed the depolarization in InAs quantum structures, e.g., islands [10], InAs/GaAs quantum dots [11–15], and single quantum well [16]. Metal nanostructures are another group that has been studied well on the (de)polarization of PL, for example, femtosecond PL depolarization of gold nanoparticles [17,18].

In the last two decades, the optical responses of the linear steep dispersion relations in electron band structures, which are present in graphene and topological materials, have been extensively studied. Photoexcited electrons and holes in these materials experience ultrafast energy relaxation owing to efficient electron-electron and electron-phonon scattering over a wide energy range. Indeed, transient reflection measurements showed that the isotropic momentum distribution of electrons in graphene, after excitation by a linearly polarized pulse, is established in less than a few hundred femtoseconds [19,20], though the depolarization of PL from graphene was not shown.

*Author to whom correspondence should be addressed: koyama@nuap.nagoya-u.ac.jp

A linearlike steep dispersion relation has also been observed in conventional bulk semiconductors. For example, in III-V semiconductors with light electron effective masses, the conduction band exhibits a linearlike steep dispersion relation over a wide energy range [21,22]. InAs is a narrow-gap III-V semiconductor with a band-gap energy of approximately 0.35 eV at 297–300 K [23], where an electron effective mass at the center of the Brillouin zone is $0.025 \times m_0$ (m_0: electron rest mass) [24]. Nansei *et al.* [25] studied the dynamics of photoexcited electrons and holes in InAs using femtosecond PL measurements. They investigated the thermalization and cooling of the carriers by observing the PL above 0.9 eV; however, no depolarization was observed.

In this study, we demonstrate the femtosecond depolarization of PL from InAs excited by linearly polarized laser pulses. To understand an essential mechanism of ultrafast depolarization, comparison among several materials is helpful. We also observe depolarization of PL from Cu and monolayer graphene, and the most effective mechanism is discussed.

II. METHODS

The samples consisted of a (111) InAs crystal, a Cu sheet (purity 99.99%, thickness 1 mm), and monolayer graphene. The Cu sheets and monolayer graphene were purchased from Nilaco and Sigma-Aldrich, respectively. The graphene was transferred onto a quartz glass substrate. We checked that PL from the quartz glass substrate was not detected. The InAs crystal was an undoped *n*-type InAs wafer. The wafer was checked by the measuring x-ray diffraction pattern (Rigaku, SmartLab, Cu $K\alpha$) and the Raman-scattering spectrum (Renishaw, inVia, He-Ne laser) at 298 K [26–28]. The inset of Fig. 1(d) shows the diffraction pattern for the x ray incident to the wafer surface, where the PL was measured. A strong peak is observed at $18.0\,\mathrm{nm}^{-1}$, which is attributed to the (111) peak of InAs ($Q = 18.0\,\mathrm{nm}^{-1}$). Figure 1(d) shows the Raman-scattering spectrum of this surface in the backscattering geometry. The spectrum shows sharp peaks at 217 and $238\,\mathrm{cm}^{-1}$, which are attributed to transverse optical (TO) and longitudinal optical (LO) modes, respectively. It is known

 ©2023 American Physical Society

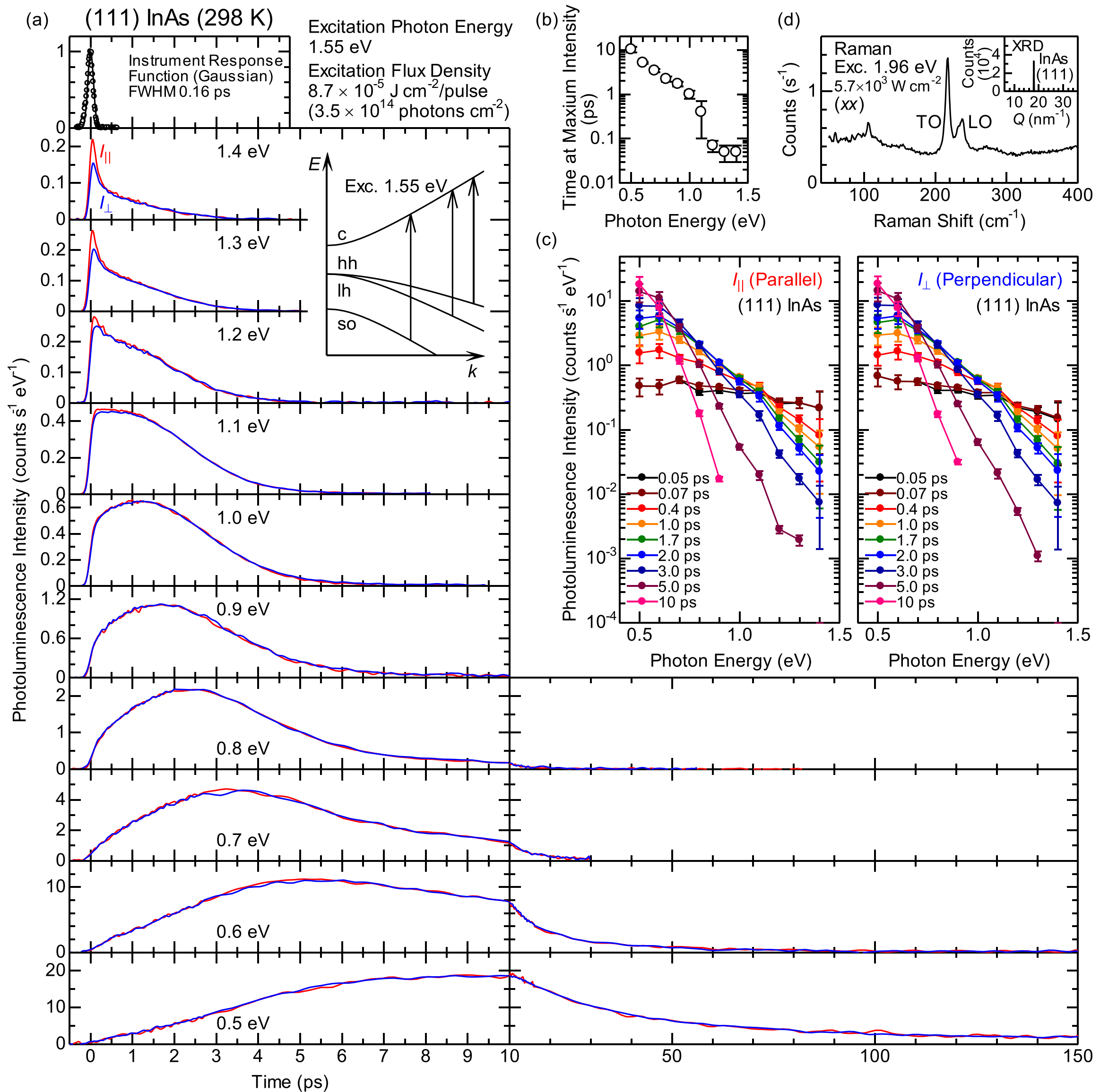

FIG. 1. (a) Time-dependent $I_{\parallel}$ (red) and $I_{\perp}$ (blue) of InAs at different photon energies. Top panel shows the instrument response function (circles) and a fitted result using a Gaussian function (black curve) with a FWHM of 0.16 ps. The inset shows a schematic of electron energy dispersions of InAs near the Brillouin zone center. Vertical arrows indicate photoexcitation of electrons. The labels c, hh, lh, and so denote conduction, heavy-hole, light-hole, and split-off bands, respectively. (b) PL photon energy dependence of time at maximum PL kinetics. (c) Time-resolved PL spectra for $I_{\parallel}$ and $I_{\perp}$ of InAs. (d) Raman-scattering spectrum of the sample in the backscattering geometry. The label (*xx*) denotes that the polarization directions of excitation and scattered lights are parallel to the *x* axis in the laboratory system. The measured surface is the same as that in the PL measurements. The peaks at 217 and 238 cm^{-1} are attributed to transverse optical (TO) and longitudinal optical (LO) modes of InAs. The inset shows an x-ray diffraction (XRD) pattern of the sample. The peak at 18.0 nm^{-1} indicates the (111) peak of InAs.

that both of them are observed in the (111) backscattering geometry [26,28], while in the spectrum of the (001) or (110) backscattering geometry, only LO or TO modes are observed, respectively [27]. Therefore, our wafer is (111) InAs crystal.

A broad component with a shoulder at $\sim$100 cm^{-1} is observed in the spectrum, while it was not present in an undoped InAs crystal with a low carrier density ($<10^{16}$ cm^{-3}) [29]. The broad component is ascribed to electronic Raman scattering involving the collective plasmon excitation, and the energy of this shoulder approximately corresponds to the plasma frequency [30]. The spectral shape of this broad component is independent of the excitation density, and its intensity is proportional to the excitation density. These spectral features indicate that the broad component is the electronic Raman signal of intrinsic carriers, not the photoexcited carriers. The plasma frequency is calculated to be 100 cm^{-1} using the carrier concentration of 4×10^{16} cm^3, the electron effective mass of $0.025 \times m_0$, and the background permittivity of 14.76 in the low-frequency region <100 cm^{-1} [31]. Thus, the roughly estimated value of carrier concentration in our InAs is $\sim 4 \times 10^{16}$ cm^3, which is consistent with a typical carrier concentration of 2×10^{16} cm^{-3} in undoped *n*-type InAs [23].

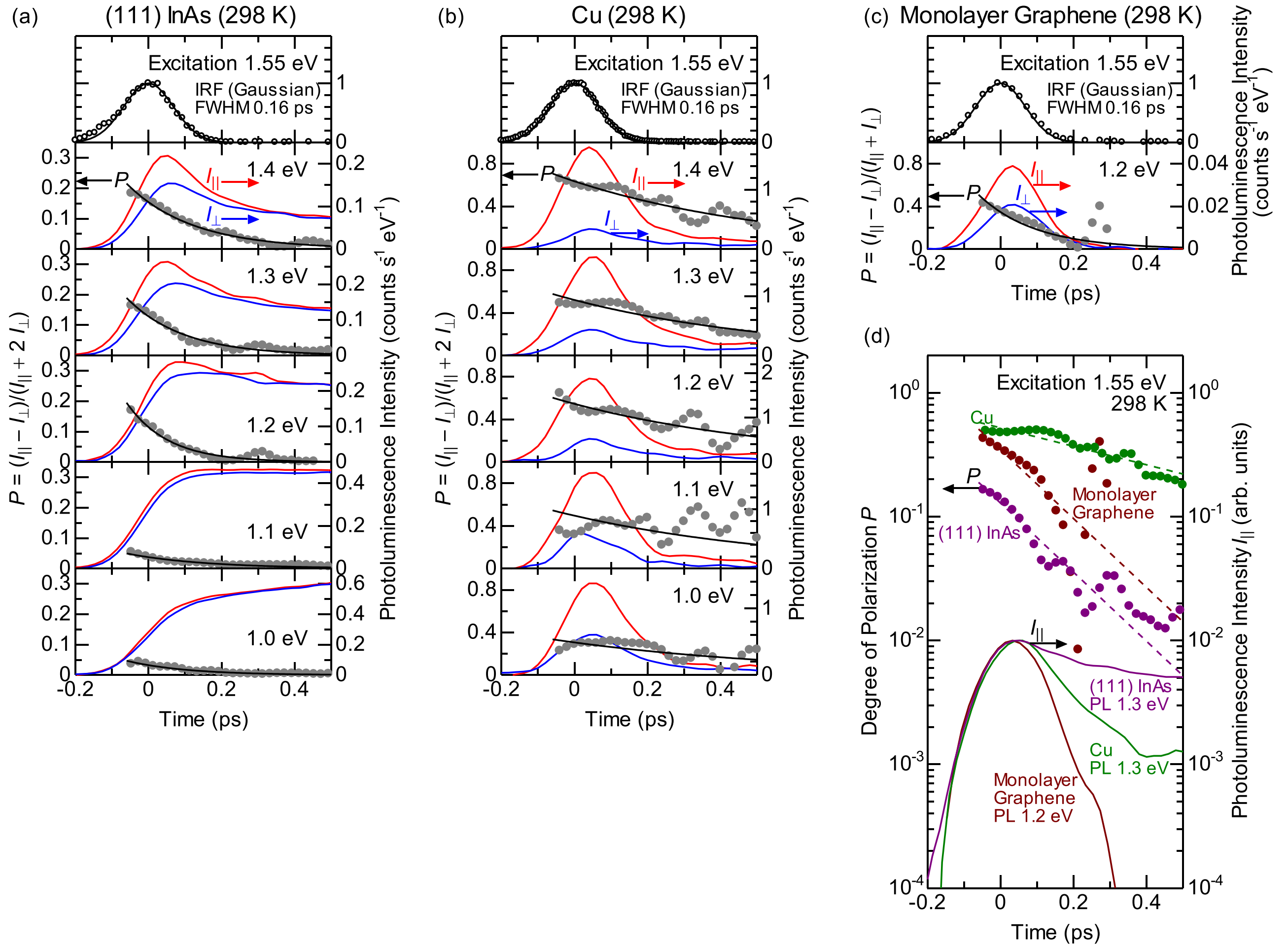

FIG. 2. Time-dependent degree of polarization P in (a) InAs, (b) Cu, and (c) monolayer graphene. Top panel shows the instrument response function (IRF; circles) and a fitted result using a Gaussian function (black curve). Below the top panel, the time dependences of P (gray circles) are shown. Black curves indicate the fitted results of the single-exponential function model. Time-dependent $I_{\parallel}$ (red) and $I_{\perp}$ (blue) are shown for comparison. (d) Comparison of time-dependent P and $I_{\parallel}$ among InAs (purple), Cu (green), and monolayer graphene (brown). Dashed curves indicate the fitted results of the single-exponential function model.

Femtosecond PL was measured using the frequency up-conversion technique [32] with a home-built measurement system [33]. A Ti:sapphire laser (800 nm, 100 fs, and 82 MHz) was used as the light pulse source. The output of the laser was divided into excitation and gate pulses using a beam splitter. The excitation pulse was passed through a variable neutral density filter, half-wave plate, and lens and focused on the sample. The spot size of the excitation pulse on the sample surface was 50 μm, and the incident excitation flux densities per pulse were 8.7×10^{-5} J cm^{-2} for InAs and Cu and 2.5×10^{-5} J cm^{-2} for graphene. The PL emitted from the sample was reflected by a pair of paraboloidal mirrors and focused on a nonlinear optical crystal (β-barium borate). After traveling on a delay stage, the gate pulse was focused on the nonlinear optical crystal as it overlapped with the PL, and the sum-frequency light between the PL and the gate pulse was generated. The sum-frequency light was directed to a monochromator and detected using a photomultiplier with a photon-counting unit. To convert the detected sum-frequency signal to PL intensity, we used the sum-frequency generation data between an infrared standard light source and a gate pulse [34,35]. All samples were measured at 298 K in air.

The instrument response functions were measured using the cross-correlation signals between the excitation pulses scattered at the sample surfaces and the gate pulse. The cross-correlation traces for InAs, Cu, and monolayer graphene are shown in the top panels of Figs. 1(a), 3(a), and 4(a), respectively, and again in the top panels of Figs. 2(a), 2(b), and 2(c), respectively. They were fitted with a Gaussian function with a full width at half maximum of 0.16 ps (black curve). This value represents the temporal resolution of the measurement system. The spectral bandwidth was determined mainly by a spectral width of gate pulse and an acceptance angle for sum-frequency generation, and the typical value was 0.02 eV. This gave the energy resolution of our measurements.

Because the sum-frequency generation in our experiment was based on the type-I phase-matching condition, the PL with polarization parallel to that of the gate pulse contributed to the sum-frequency generation. In other words, the PL polarization direction was selected based on sum-frequency

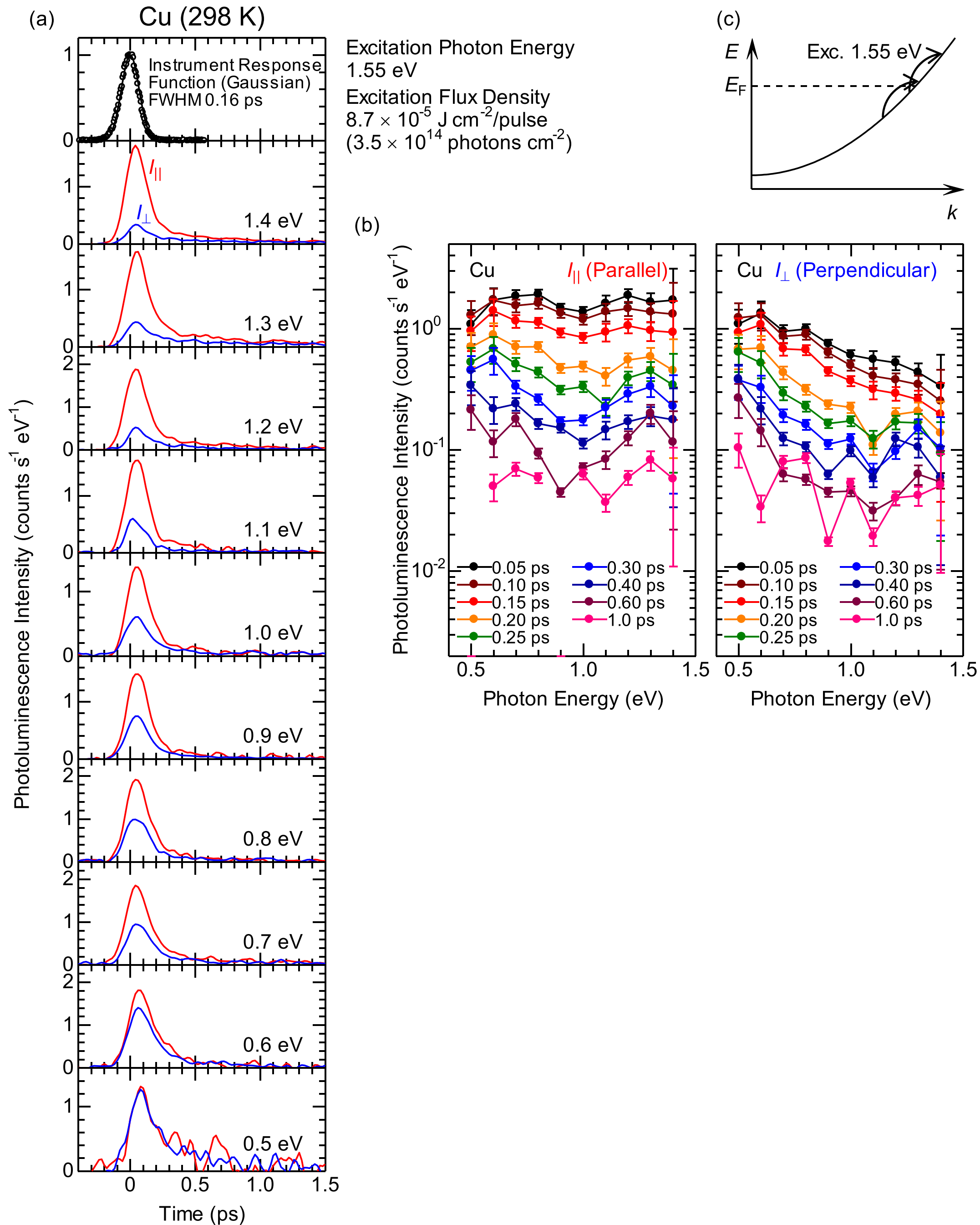

FIG. 3. (a) Time-dependent $I_{\parallel}$ (red) and $I_{\perp}$ (blue) of Cu at different photon energies. Top panel shows the instrument response function (circles) and a fitted result using a Gaussian function (black). (b) Time-resolved PL spectra for $I_{\parallel}$ and $I_{\perp}$ of Cu. (c) Schematic of electron energy dispersion of Cu. Arc arrows indicate typical intraband excitation of electrons by photoabsorption in this study.

generation. In our experiment, the gate polarization was fixed, and the excitation polarization was set parallel or perpendicular to it by adjusting the half-wave plate. The accuracy of the polarization detection was tested by measuring the cross-correlation signals between the gate pulse and the excitation pulses with parallel and perpendicular polarization. The ratio of the signal intensity was 0.02, which gave the polarization detection accuracy of the measurement system.

In this paper, the PL intensities are denoted by $I_{\parallel}$ and $I_{\perp}$ for the excitation polarization parallel and perpendicular to the gate polarization, respectively. The incidence was not exactly perpendicular to the sample for the measurements of $I_{\parallel}$ and $I_{\perp}$, because the excitation pulse was directed to the sample as the *s*- and *p*-polarized lights, respectively, resulting in the different reflectivity and absorptivity. For InAs, the excitation polarizations for $I_{\parallel}$ and $I_{\perp}$ are parallel to $[11\bar{2}]$ and $[\bar{1}10]$, respectively. The powers of the incident and reflected excitation pulses were measured to obtain the reflectivity for each polarization. In addition, a slight temporal change in the laser output power was considered. The values of $I_{\perp}$ were

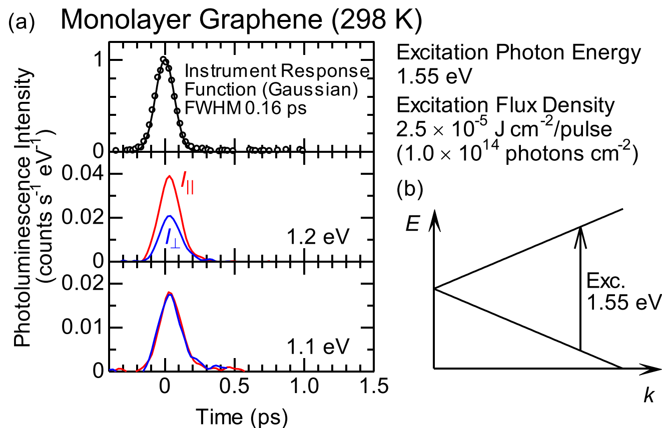

FIG. 4. (a) Time-dependent $I_{\parallel}$ (red) and $I_{\perp}$ (blue) of monolayer graphene at 1.1 and 1.2 eV. Top panel shows the instrument response function (circles) and the fitted result using a Gaussian function (black). (b) Schematic of electron energy dispersion of monolayer graphene near the K point. Vertical arrow indicates photoexcitation of electrons.

multiplied by the constants and normalized by the absorbed flux density.

III. RESULTS AND DISCUSSION

Figure 1(a) shows the time-dependent $I_{\parallel}$ of InAs at different photon energies from 0.5 to 1.4 eV (red curves). The excitation pulse creates electrons in the first conduction band, heavy and light holes, and holes in the split-off band in the vicinity of the Brillouin zone center as schematically shown in the inset of Fig. 1(a). At 1.2, 1.3, and 1.4 eV, steep increases and decreases in PL intensity are observed until 0.4 ps. The same PL component was observed in the early study by Nansei *et al.* [25], where it was attributed to nonthermal electrons. A long-decay component is superimposed on this steep PL component. As the detection photon energy decreases, the PL kinetics show a slow increase and a longer-decay behavior. This behavior indicates relaxation of the electron and hole distributions, and the early experiment by Nansei *et al.* [25] showed the similar decay behavior above 0.9 eV.

The time at which each PL kinetic reaches a maximum is shown in Fig. 1(b). The time difference between neighboring points increases toward low photon energies, indicating that the relaxation of the distributions slows at low energies because of the small density of states and low cooling rate. The left panel of Fig. 1(c) shows the time-resolved PL spectra for $I_{\parallel}$. The PL intensity on the high-energy side decreases with time, whereas that on the low-energy side increases. Hence, the spectral shape becomes sharp, and the center of the spectral weight moves to a lower energy, showing the relaxation of the electron and hole distributions.

The PL component at low energy observed around the time origin suggests the rapid formation of electron and hole distributions in the low-energy regions by impact ionization and scattering between photoexcited electrons, which start just after excitation within the time resolution. In the impact ionization, a valence-band electron (conduction-band hole) is excited to a conduction (valence) band by interacting with a photoexcited electron (hole) to compensate for the excess energy. Early studies have shown that efficient electron-impact ionization occurs in InAs [36–38]. This ionization populates electrons in the vicinity of the bottom of the conduction band, and they contribute to the finite PL at 0.5 and 0.6 eV in the early part of our experiment.

The first conduction band in zinc-blende materials possesses a linearlike dispersion over a wide energy range owing to interband interaction [39]. In our experiment, photoexcitation populated the electrons in a linearlike dispersion of InAs. Scattering between the photoexcited electrons in the linearlike dispersion can satisfy energy and momentum conservation over a wide energy range. Hence, this scattering results in a broad energy distribution of electrons. In fact, the hot luminescence of InAs excited by 780-nm light was observed even at 400 nm in the ultraviolet region [40], the origin of which might be electron distribution formed by the excitation of photoexcited electrons by scattering among them on the linearlike dispersion. The counterparts of the scattered photoexcited electrons relax to the low-energy region. Such relaxed photoexcited electrons are involved in the finite PL at 0.5 and 0.6 eV in the early part of our experiment. Similar wide-range scattering of photoexcited electrons and holes has been observed in graphene with a linear dispersion [41]. The relatively strong PL at low energy even at 0.02 ps is partially because the transition matrix element is large toward the zone center in zinc-blende materials [21,42].

Figure 1(a) (blue curves) and the right side of Fig. 1(c) show the time-dependent $I_{\perp}$ of InAs and the time-resolved spectra, respectively. Although the decay behavior of $I_{\perp}$ is approximately the same as that of $I_{\parallel}$ at the corresponding energies, the PL intensities of $I_{\perp}$ at 1.4, 1.3, 1.2, 1.1, and 1.0 eV are low until 0.4 ps. This difference indicates an anisotropic momentum distribution of the electrons. The distribution becomes isotropic when $I_{\perp}$ and $I_{\parallel}$ coincide and the depolarization is complete. Depolarization is almost complete at 0.4 ps.

To examine the depolarization dynamics in InAs, the degree of polarization P is defined by $(I_{\parallel} - I_{\perp})/(I_{\parallel} + 2I_{\perp})$ and shown in Fig. 2(a) (gray circles) with $I_{\parallel}$ (red) and $I_{\perp}$(blue). The maximum value of P is observed at 1.4 eV and -0.05 ps, and the value is 0.18, which is much less than 1. Early studies [43] showed momentum distribution functions of electrons and holes generated by a linearly polarized light excitation in GaAs-type semiconductors. For the excitation from the heavy hole to the conduction band, the selection rule determines that electrons and holes have momenta directed predominantly normal to the excitation polarization, and no electrons or holes have momenta directed along the excitation polarization. In contrast, for the excitation from the light hole to the conduction band, a large part of electrons and holes have momenta directed along the excitation polarization, and a small part of electrons and holes have momenta directed normal to the excitation polarization. The radiative recombination of an electron and a hole is governed by the same selection rules. Therefore, for the recombination of the electron and hole created by the linearly polarized light excitation from the light hole to the conduction band, it is possible to emit PL with a polarization perpendicular to the excitation polarization even before polarization relaxation. This causes low P. In addition, the linearly

TABLE I. Fitted values of depolarization time constant in InAs, Cu, and monolayer graphene.

Photon energy (eV)	Depolarization time constant τ (ps)		
	InAs	Cu	Monolayer graphene
1.4	0.18 ± 0.01	0.56 ± 0.05	
1.3	0.16 ± 0.01	0.58 ± 0.05	
1.2	0.11 ± 0.01	0.60 ± 0.08	0.16 ± 0.02
1.1	0.22 ± 0.02	0.6 ± 0.2	
1.0	0.16 ± 0.01	0.7 ± 0.2	

polarized light excitation from the split-off band to the conduction band generates isotropic momentum distributions of electrons and holes [43]. The PL emitted by a recombination of these electrons and holes is nonpolarized, resulting in lower P. The early calculation [43] showed that $P = 2/13 \sim 0.154$ for the linearly polarized excitation light incident on a GaAs crystal in the [111] direction, and this value is independent of the excitation polarization. This calculation agrees well with the experiments on steady-state hot luminescence of GaAs [44]. These studies are consistent with our low value of P.

The initial value of P decreases toward lower energies. This indicates that energy relaxation proceeds with depolarization at the time resolution. The curve P above 1.0 eV at each photon energy shows a monotonous decrease by approximately 0.5 ps within the error, and it is phenomenologically fitted with a single exponential function $\propto \exp(-t/\tau)$ with a depolarization time constant τ using the data in the range of −0.05–0.50 ps. The experimental results are reproduced well in Fig. 2(a) (black curves), and the obtained values of τ are listed in Table I. The mean value of τ is 0.17 ± 0.01 ps, and this is the depolarization time constant in InAs. The early study by Boggess *et al.* [45] determined a momentum relaxation time of 0.34 ps, which is comparable to the depolarization time constant of 0.17 ± 0.01 ps in our study.

Here, we discuss the possible origins of ultrafast depolarization in InAs. First is electron-electron scattering among the photoexcited electrons and holes. The concentrations of photoexcited electrons and holes in our experiments were estimated to be $\sim 2 \times 10^{19}$ cm^{-3} using an absorbed flux density of 2.5×10^{14} photons cm^{-2} per pulse and an absorption coefficient of $\sim 7 \times 10^4$ cm^{-1} [46]. (The concentration might be lower than this value owing to absorption saturation.) A high carrier concentration leads to a high scattering rate, resulting in the quick formation of an isotropic distribution of electrons and holes. (The estimated intrinsic carrier concentration in our InAs is $\sim 4 \times 10^{16}$ cm^{-3} and negligible compared with the photoexcited electrons and holes.)

Second is another electron-electron scattering, impact ionization. As described above, InAs has a narrow gap and high impact ionization efficiency [36–38]. This ionization causes the randomization of the electron and hole distributions.

Third is electron-optical phonon scattering, which is accelerated by a steep electron energy dispersion. The linearlike dispersion in the first conduction band of InAs is steep [22,39], which enables photoexcitation to create electrons and holes near the center of the Brillouin zone, despite the high excitation photon energy. These photoexcited electrons and holes can be scattered by phonons with small wavenumbers, which causes randomization of the distributions of electrons and holes. Owing to the strong Frölich interaction [47] and high density of states of optical phonons [48] near the zone center, the scattering rate of photoexcited electrons and holes by these phonons is high, and an isotropic distribution of electrons and holes can be established quickly.

The PL kinetics of Cu were investigated to determine the most effective of these three options. Cu is a simple metal with a large number of carriers (1.2×10^{23} cm^{-3}) [49,50], and Auger recombination of photoexcited carriers occurs efficiently [51,52]. Hence, Cu is a suitable reference material for studying the first and second options (electron-electron scattering). In addition, considering the band structure of Cu [53], we attributed the photoexcitation of Cu to the intraband excitation of electrons across the Fermi energy as illustrated in Fig. 3(c). In other words, photoexcitation populates the excited electrons and holes at large wavenumbers. Thus, Cu is also an appropriate reference for the third option (electron-optical phonon scattering accelerated by a steep energy dispersion).

Figure 3(a) shows time-dependent $I_{\parallel}$ (red) and $I_{\perp}$ (blue) of Cu at different photon energies from 0.5 to 1.4 eV. The time-resolved PL spectra for $I_{\parallel}$ and $I_{\perp}$ are shown in Fig. 3(b). For all the detection photon energies, the PL kinetics show very fast decay behavior, and the PL intensity decreases to almost zero within 1.5 ps. At 1.4 eV, the maximum intensity of $I_{\parallel}$ is approximately four times higher than that of $I_{\perp}$. The difference between $I_{\parallel}$ and $I_{\perp}$ decreases toward lower energies. At 0.5 eV, $I_{\parallel}$ and $I_{\perp}$ show the same decay curve, and the depolarization is complete until the electron population relaxes to the corresponding energy region. Time-dependent P is plotted as gray circles in Fig. 2(b). The decay of P is slower than that of PL. This indicates that the energy relaxation largely proceeds independently of depolarization, whereas the gradual decrease in the initial value of P toward low energy indicates the presence of a small part of the energy relaxation with depolarization. The curves for P are fitted with a single exponential function, and the obtained values of τ are listed in Table I. The mean value of τ is 0.6 ± 0.1 ps, and the depolarization time constant obtained is 0.6 ± 0.1 ps. This value is higher than the depolarization time constant of 0.17 ps in InAs. The comparison of the time-dependent P and $I_{\parallel}$ between InAs and Cu is clearly shown in Fig. 2(d). The decay of P at 1.3 eV of InAs (purple) is faster than that of Cu (green), whereas the decay of $I_{\parallel}$ of InAs is slower than that of Cu. Thus, depolarization is faster in InAs than in Cu, and the first and second options are (probably effective, but) not the most effective, for ultrafast depolarization in InAs. The residual third option of electron-optical phonon scattering accelerated by steep energy dispersion, is the most effective.

The scattering rate is proportional to the absolute square of the matrix element of the interaction Hamiltonian. For the electron-phonon interactions in metals [54] as well as polar semiconductors (Frölich interaction) [55], the absolute square of the matrix element is proportional to $(q^2 + k_s^2)^{-1}$, where q is the phonon wave vector and k_s is the screening wave vector. The wave number of optical phonons strongly contributing to the depolarization has a similar value to that of the photoexcited electrons, the typical value of which is in the order

of a magnitude of 1 and $10\,\mathrm{nm}^{-1}$ in InAs [22] and Cu [53], respectively. The value of k_s is in the order of the Fermi wave number and $< \sim 1\,\mathrm{nm}^{-1}$ in InAs and $\sim 10\,\mathrm{nm}^{-1}$ in Cu. Thus, the electron-phonon scattering rate is roughly ~ 100 times higher in InAs. In contrast, the depolarization rate (inverse of depolarization time) in InAs is only four times higher than that in Cu. This is probably because the electron-electron scattering largely contributes to the depolarization in Cu.

Finally, a general view of this interpretation is examined. A typical material with steep energy dispersion is monolayer graphene, where linear dispersions are present in the vicinity of the K point as schematically shown in Fig. 4(b). Figure 4(a) shows the time-dependent $I_{\parallel}$ (red) and $I_{\perp}$ (blue) of the monolayer graphene at 1.1 and 1.2 eV. At 1.2 eV, $I_{\perp}$ is smaller than $I_{\parallel}$, while $I_{\perp}$ is the same as $I_{\parallel}$ within the error at 1.1 eV. The degree of polarization P is redefined by $(I_{\parallel} - I_{\perp})/(I_{\parallel} + I_{\perp})$ for two-dimensional materials and is plotted with gray circles in Fig. 2(c). Curve P (1.2 eV) was fitted with a single exponential function, and the depolarization time constant obtained is 0.16 ± 0.02 ps (Table I). This value is consistent with the results of previous transient reflection experiments [19,20]. The establishment of an isotropic momentum distribution of electrons in graphene by scattering optical phonons around the zone center has been shown in a theoretical study [56]. Figure 2(d) shows that the decay of P at 1.3 eV of InAs (purple) is as fast as that at 1.2 eV of monolayer graphene (brown). The depolarization times in InAs and monolayer graphene are consistent despite the different materials, indicating that ultrafast depolarization is a characteristic of materials with steep energy dispersion.

IV. CONCLUSION

In this study, we measured the femtosecond PL of InAs, Cu, and monolayer graphene excited by linearly polarized laser pulses. The degree of polarization was calculated for the three materials and fitted to a single exponential function. The depolarization time constants obtained for InAs, Cu, and monolayer graphene were 0.17 ± 0.01, 0.6 ± 0.1, and 0.16 ± 0.02 ps, respectively. Depolarization is discussed in terms of the electron-electron and electron-phonon scattering. A steep dispersion relation in the electron band structure accelerates the electron-optical phonon scattering causing the ultrafast depolarization of PL. This study indicates that ultrafast depolarization is a characteristic of materials with steep energy dispersion.

ACKNOWLEDGMENT

This work was supported by Shorai Foundation for Science and Technology.

[1] See, for example, *Optical Orientation*, edited by F. Meier and B. P. Zakharchenya (North-Holland, Amsterdam, 1984).

[2] J. M. Kikkawa, I. P. Smorchkova, N. Samarth, and D. D. Awschalom, Room-temperature spin memory in two-dimensional electron gases, Science **277**, 1284 (1997).

[3] B. P. Zakharchenya, D. N. Mirlin, V. I. Perel, and I. I. Reshina, Spectrum and polarization of hot-electron photoluminescence in semiconductors, Sov. Phys. Usp. **25**, 143 (1982).

[4] R. C. Miller and D. A. Kleinman, Excitons in GaAs quantum wells, J. Lumin. **30**, 520 (1985).

[5] R. Sooryakumar, D. S. Chemla, A. Pinczuk, A. C. Gossard, W. Wiegmann, and L. J. Sham, Valence band mixing in GaAs-(AlGa)As heterostructures, Solid State Commun. **54**, 859 (1985).

[6] M. J. Snelling, A. S. Plaut, G. P. Flinn, A. C. Tropper, R. T. Harley, and T. M. Kerr, Spin relaxation in optically excited quantum wells, J. Lumin. **45**, 208 (1990).

[7] H. Stolz, D. Schwarze, W. von der Osten, and G. Weimann, Transient optical alignment and relaxation of excitons in GaAs/AlGaAs quantum wells, Superlattices Microstruct. **6**, 271 (1989).

[8] T. C. Damen, K. Leo, J. Shah, and J. E. Cunningham, Spin relaxation and thermalization of excitons in GaAs quantum wells, Appl. Phys. Lett. **58**, 1902 (1991).

[9] T. C. Damen, L. Viña, J. E. Cunningham, J. Shah, and L. J. Sham, Subpicosecond spin relaxation dynamics of excitons and free carriers in GaAs quantum wells, Phys. Rev. Lett. **67**, 3432 (1991).

[10] B. Salem, J. Olivares, J. Brault, C. Monat, M. Gendry, G. Hollinger, H. Maaref, G. Guillot, and G. Bremond, Optical anisotropy and photoluminescence temperature dependence for self-assembled InAs quantum islands grown on vicinal (001) InP substrates, Microelecton. J. **33**, 579 (2002).

[11] M. Paillard, X. Marie, P. Renucci, T. Amand, A. Jbeli, and J. M. Gérard, Spin relaxation quenching in semiconductor quantum dots, Phys. Rev. Lett. **86**, 1634 (2001).

[12] R. J. Epstein, D. T. Fuchs, W. V. Schoenfeld, P. M. Petroff, and D. D. Awschalom, Hanle effect measurements of spin lifetimes in InAs self-assembled quantum dots, Appl. Phys. Lett. **78**, 733 (2001).

[13] V. K. Kalevich, M. Paillard, K. V. Kavokin, X. Marie, A. R. Kovsh, T. Amand, A. E. Zhukov, Yu. G. Musikhin, V. M. Ustinov, E. Vanelle, and B. P. Zakharchenya, Spin redistribution due to Pauli blocking in quantum dots, Phys. Rev. B **64**, 045309 (2001).

[14] S. Cortez, O. Krebs, S. Laurent, M. Senes, X. Marie, P. Voisin, R. Ferreira, G. Bastard, J.-M. Gérard, and T. Amand, Optically driven spin memory in *n*-doped InAs-GaAs quantum dots, Phys. Rev. Lett. **89**, 207401 (2002).

[15] P.-F. Braun, X. Marie, L. Lombez, B. Urbaszek, T. Amand, P. Renucci, V. K. Kalevich, K. V. Kavokin, O. Krebs, P. Voisin, and Y. Masumoto, Direct observation of the electron spin relaxation induced by nuclei in quantum dots, Phys. Rev. Lett. **94**, 116601 (2005).

[16] O. Brandt, H. Lage, and K. Ploog, Heavy- and light-hole character of optical transitions in InAs/GaAs single-monolayer quantum wells, Phys. Rev. B **45**, 4217 (1992).

[17] O. Varnavski, R. G. Ispasoiu, L. Balogh, D. Tomalia, and T. Goodson, III, Ultrafast time-resolved photoluminescence from

novel metal-dendrimer nanocomposites, J. Chem. Phys. **114**, 1962 (2001).
[18] O. P. Varnavski, T. Goodson, III, M. B. Mohamed, and M. A. El-Sayed, Femtosecond excitation dynamics in gold nanospheres and nanorods, Phys. Rev. B **72**, 235405 (2005).
[19] M. Mittendorff, T. Winzer, E. Malic, A. Knorr, C. Berger, W. A. de Heer, H. Schneider, M. Helm, and S. Winnerl, Anisotropy of excitation and relaxation of photogenerated charge carriers in graphene, Nano Lett. **14**, 1504 (2014).
[20] J. Yao, X. Zhao, X.-Q. Yan, C. Gao, X.-D. Chen, W. Xin, Y. Chen, Z.-B. Liu, and J.-G. Tian, Polarization dependence of optical pump-induced change of graphene extinction coefficient, Opt. Mater. Express **5**, 1550 (2015).
[21] For an example of InSb, see E. O. Kane, Band structure of indium antimonide, J. Phys. Chem. Solids **1**, 249 (1957).
[22] Y.-S. Kim, M. Marsman, G. Kresse, F. Tran, and P. Blaha, Towards efficient band structure and effective mass calculations for III-V direct band-gap semiconductors, Phys. Rev. B **82**, 205212 (2010).
[23] S. T. Schaefer, S. Gao, P. T. Webster, R. R. Kosireddy, and S. R. Johnson, Absorption edge characteristics of GaAs, GaSb, InAs, and InSb, J. Appl. Phys. **127**, 165705 (2020).
[24] D. Long, Energy band structures of mixed crystals of III–V compounds, in *Physics of III–V Compounds*, edited by R. K. Willardson and A. C. Beer, Semiconductors and Semimetals (Academic, New York, 1966), Vol. 1, Chap. 5, p. 143.
[25] H. Nansei, S. Tomimoto, S. Saito, and T. Suemoto, Femtosecond luminescence from partly redistributed nonequilibrium electrons in InAs, Phys. Rev. B **59**, 8015 (1999).
[26] M. Möller, M. M. de Lima, Jr., A. Cantarero, L. C. O. Dacal, J. R. Madureira, F. Iikawa, T. Chiaramonte, and M. A. Cotta, Polarized and resonant Raman spectroscopy on single InAs nanowires, Phys. Rev. B **84**, 085318 (2011).
[27] H. Liu, Y. Zhang, E. H. Steenbergen, S. Liu, Z. Lin, Y.-H. Zhang, J. Kim, M.-H. Ji, T. Detchprohm, R. D. Dupuis, J. K. Kim, S. D. Hawkins, and J. F. Klem, Raman scattering study of lattice vibrations in the type-II superlattice InAs/$InAs_{1-x}Sb_x$, Phys. Rev. Appl. **8**, 034028 (2017).
[28] J. H. Park and C.-H. Chung, Raman spectroscopic characterizations of self-catalyzed InP/InAs/InP one-dimensional nanostructures on InP(111)B substrate using a simple substrate-tilting method, Nanoscale Res. Lett. **14**, 355 (2019).
[29] R. Carles, N. Saint-Cricq, J. B. Renucci, A. Zwick, and M. A. Renucci, Resonance Raman scattering in InAs near the E_1 edge, Phys. Rev. B **22**, 6120 (1980).
[30] B. H. Bairamov, I. P. Ipatova, and V. A. Voitenko, Raman scattering from current carriers in solids, Phys. Rep. **229**, 221 (1993).
[31] R. Mendis, M. L. Smith, L. J. Bignell, R. E. M. Vickers, and R. A. Lewis, Strong terahertz emission from (100) *p*-type InAs, J. Appl. Phys. **98**, 126104 (2005).
[32] J. Shah, Ultrafast luminescence spectroscopy using sum frequency generation, IEEE J. Quantum Electron. **24**, 276 (1988).
[33] T. Koyama, Y. Miyata, K. Asaka, H. Shinohara, Y. Saito, and A. Nakamura, Ultrafast energy transfer of one-dimensional excitons between carbon nanotubes: A femtosecond time-resolved luminescence study, Phys. Chem. Chem. Phys. **14**, 1070 (2012).
[34] K. Saito, T. Koishi, J. Bao, W. Norimatsu, M. Kusunoki, H. Kishida, and T. Koyama, Photoluminescence enhancement exceeding 10-fold from graphene via an additional layer: Photoluminescence from monolayer and bilayer graphene epitaxially grown on SiC, J. Phys. Chem. C **125**, 11014 (2021).
[35] T. Koyama, N. Umewaki, K. Saito, T. Tatsuno, A. Fujisaki, Y. Miyata, H. Kataura, and H. Kishida, Photoluminescence of metallic single-walled carbon nanotubes: Role of interband and intraband transitions, Phys. Rev. B **106**, 045421 (2022).
[36] A. R. J. Marshall, C. H. Tan, M. J. Steer, and J. P. R. David, Electron dominated impact ionization and avalanche gain characteristics in InAs photodiodes, Appl. Phys. Lett. **93**, 111107 (2008).
[37] A. R. J. Marshall, J. P. R. David, and C. H. Tan, Impact ionization in InAs electron avalanche photodiodes, IEEE Trans. Electron. Dev. **57**, 2631 (2010).
[38] I. C. Sandall, J. S. Ng, S. Xie, P. J. Ker, and C. H. Tan, Temperature dependence of impact ionization in InAs, Opt. Express **21**, 8630 (2013).
[39] E. O. Kane, The $\mathbf{k} \cdot \mathbf{p}$ method, in *Physics of III-V Compounds*, edited by R. K. Willardson and A. C. Beer, Semiconductors and Semimetals (Academic, New York, 1966), Vol. 1, Chap. 3, p. 75.
[40] N. Wada, A. C. H. Rowe, and S. A. Solin, Anti-stokes and stokes hot luminescence from bulk InAs and InSb, AIP Conf. Proc. **772**, 135 (2005).
[41] T. Koyama, K. Mizutani, H. Ago, and H. Kishida, Two-step excitation triggered by one-photon absorption on linear dispersion in monolayer graphene, J. Phys. Chem. C **120**, 11225 (2016).
[42] E. J. Johnson, Absorption near the fundamental edge, in *Optical Properties of III-V Compounds*, edited by R. K. Willardson and A. C. Beer, Semiconductors and Semimetals (Academic, New York, 1967), Vol. 3, Chap. 6, p. 153.
[43] D. N. Mirlin, Optical alignment of electron momenta in GaAs-type semiconductors, in *Optical Orientation*, edited by F. Meier and B. P. Zakharchenya (North-Holland, Amsterdam, 1984), Chap. 4, p. 133, and references therein. In this article, P is defined by $(I_\parallel - I_\perp)/(I_\parallel + I_\perp)$.
[44] D. N. Mirlin and I. I. Reshina, Anisotropy of the polarization of hot photoluminescence in gallium arsenide crystals, ZhETF **73**, 859 (1977) [Sov. Phys. JETP **46**, 451 (1977)].
[45] T. F. Boggess, J. T. Olesberg, C. Yu, M. E. Flatté, and W. H. Lau, Room-temperature electron spin relaxation in bulk InAs, Appl. Phys. Lett. **77**, 1333 (2000).
[46] D. E. Aspnes and A. A. Studna, Dielectric functions and optical parameters of Si, Ge, GaP, GaAs, GaSb, InP, InAs, and InSb from 1.5 to 6.0 eV, Phys. Rev. B **27**, 985 (1983).
[47] H. Frölich, Electrons in lattice fields, Adv. Phys. **3**, 325 (1954).
[48] L. Lindsay, D. A. Broido, and T. L. Reinecke, *Ab initio* thermal transport in compound semiconductors, Phys. Rev. B **87**, 165201 (2013).
[49] T. G. Berlincourt, Hall effect, magnetoresistance, and size effects in copper, Phys. Rev. **112**, 381 (1958).
[50] J. E. Alderson, T. Farrell, and C. M. Hurd, Hall coefficients of Cu, Ag, and Au in the range 4.2–300 °K, Phys. Rev. **174**, 729 (1968).
[51] H. Petek, H. Nagano, M. J. Weida, and S. Ogawa, The role of Auger decay in hot electron excitation in copper, Chem. Phys. **251**, 71 (2000).

[52] R. Knorren, G. Bouzerar, and K. H. Bennemann, Dynamics of excited electrons in copper: The role of Auger electrons, Phys. Rev. B **63**, 094306 (2001).

[53] V. N. Strocov, R. Claessen, G. Nicolay, S. Hüfner, A. Kimura, A. Harasawa, S. Shin, A. Kakizaki, H. I. Starnberg, P. O. Nilsson, and P. Blaha, Three-dimensional band mapping by angle-dependent very-low-energy electron diffraction and photoemission: Methodology and application to Cu, Phys. Rev. B **63**, 205108 (2001).

[54] See, for example, N. W. Ashcroft and N. D. Mermin, *Solid State Physics* (Saunders College, CBS Publishing Asia, Hong Kong, 1988), p. 523.

[55] D. Kim and P. Y. Yu, Hot-electron relaxations and hot phonons in GaAs studied by subpicosecond Raman scattering, Phys. Rev. B **43**, 4158 (1991).

[56] E. Malic, T. Winzer, E. Bobkin, and A. Knorr, Microscopic theory of absorption and ultrafast many-particle kinetics in graphene, Phys. Rev. B **84**, 205406 (2011).